Investigations into the Photophysical and Electronic Properties of Pnictoles and Their Pnictenium Counterparts

Darren M. C. Ould, Alex C. Rigby, Lewis C. Wilkins, Samuel J. Adams, James A. Platts, Simon J. A. Pope, Emma Richards and Rebecca L. Melen*

School of Chemistry, Cardiff University, Main Building, Cardiff, CF10 3AT, Cymru/Wales, U.K.

ABSTRACT: The reaction of phosphole/arsole starting materials with a series of halide abstraction reagents afforded their respective phosphenium/arsenium complexes. UV-vis absorption and luminescence studies on these cations showed interesting emission profiles, which was found to be dependent upon counterion choice. The addition of a reductant to the phosphole reagent garnered a dimeric species with a central P–P bond, which when heated was found to undergo homolytic bond cleavage to produce an 11π radical complex. Electron paramagnetic resonance (EPR), supported by density functional theory (DFT) calculations, was used to characterize this radical species.

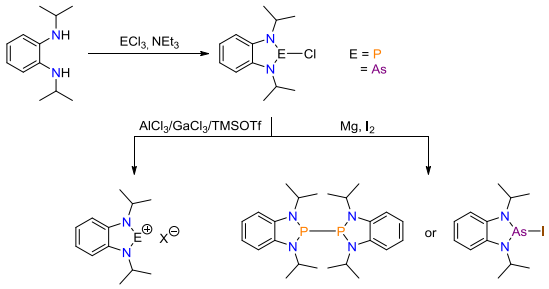

INTRODUCTION

Whilst N-heterocyclic carbenes (NHCs) have seen widespread utilization in many areas of synthetic chemistry over the past decade, their phosphorus congeners have received markedly less attention despite their presence in the literature for over half a century.[1] Even though N-heterocyclic phospheniums (NHPs) display similar characteristics to NHCs, some differences are apparent such as their enhanced π-acceptor ability and reduced σ-donor character.[2] This has led to uses as transition metal ligands with some of the most recent reports providing NHPs as ligands to group 9 and 10 metals which had previously been considered to be incompatible.[3] The above statements are also true for the analogous arsenic species, in that arsoles may be used to synthesize arsenium cations. However, like their phosphorus counterparts, these have received even less attention. Nevertheless, examples of arsenium cations are known, with Cowley and Burford being early leaders in the field.[4]

Although less well reported than phosphenium chemistry, diphosphines have recently received attention from a number of different groups due to their propensity to undergo thermally induced homolytic bond cleavage to form radical species.[5] In recent work, Wright has reported a series of $[(CH)_2(NR)_2P]_2$ dimeric complexes that underwent thermal dissociation to form 7π radical species, with the ease of radical formation increasing with the length of the P–P bond.[6] Whilst structural analyses of many of this class of compound have been seen in the literature, more detailed photophysical spectroscopic studies have been noticeably rare.

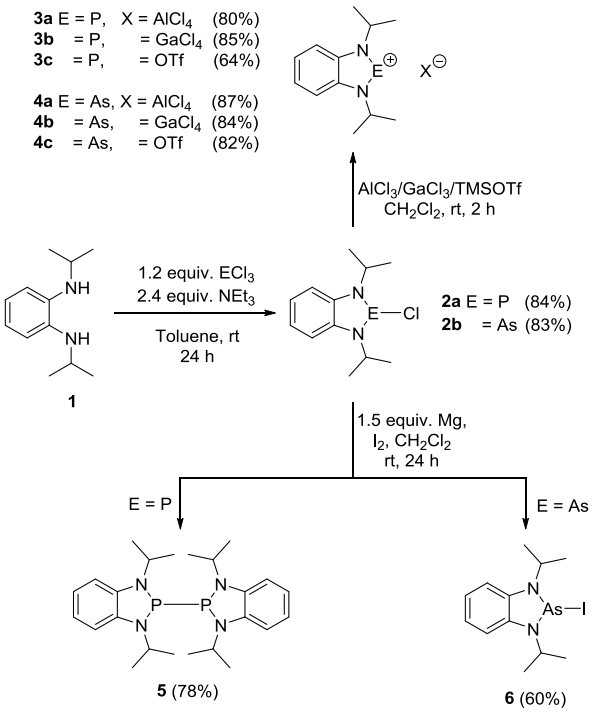

Scheme 1. Synthetic overview of this work.

In this work, the previously unreported phosphole and arsole with an *N*,*N*'-diisopropylbenzene diamine backbone were synthesized. These were then converted to the cationic phosphenium/arsenium complexes through halide abstraction as well as undergoing reduction to form dimers.

Several techniques were utilized in probing these structures, including X-ray crystallography, UV-vis spectroscopy as well as electron paramagenic resonance (EPR) spectroscopy. Furthermore, all findings were supported with density functional theory (DFT) calculations.

Results and Discussion

Initial work focused on synthesizing the pnictoles 2-chloro-1,3-diisopropyl-benzodiaza-phosphole (**2a**) and 2-chloro-1,3-diisopropyl-benzodiaza-arsole (**2b**) through the addition of *N*,*N*'-diisopropylbenzene-1,2-diamine **1** to PCl_3 or $AsCl_3$ respectively (Figure 1).

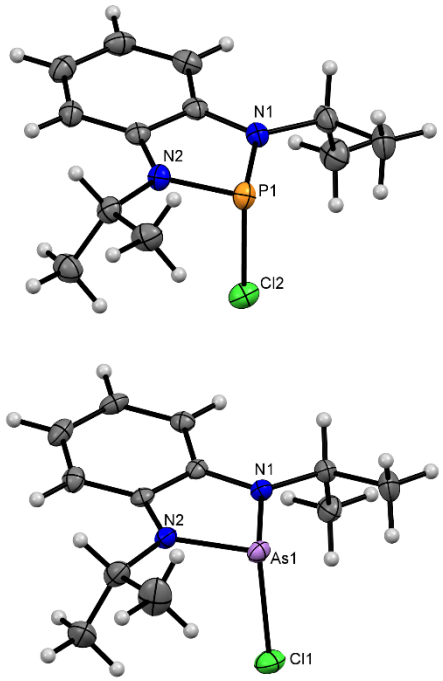

Figure 1. Solid-state structure of **2a** (top) and **2b** (bottom). Thermal ellipsoids drawn at 50% probability.

Single crystal X-ray diffraction analysis of both **2a** and **2b** revealed Pn–Cl bond lengths of 2.3378(7) Å and 2.4440(10) Å respectively. These are comparable to Pn–Cl bond lengths in similar systems reported previously.[7] In addition, the C_2N_2 unit in **2a** has C–N bond lengths of 1.403(2)–1.405(2) Å, which are just shorter than a typical C–N bond (1.47 Å),[8] and C–N–P interior bond angles of 113.09(13)°–113.48(13)°. **2b** is similar, with C–N bond lengths of 1.390(5)–1.394(5) and C–N–As interior bond angles of 113.4(2)°–113.9(2)°. To explain these observations, natural bond orbital (NBO) analyses was conducted. For **2a**, the hybrid functional B3LYP and 6-31+G(2d,p) basis set was employed,[9] with the natural population analysis showing a large build-up of positive charge on the phosphorus atom and negative charge on the chloride atom (1.273 and -0.593 respectively), suggesting the P–Cl bond is highly polarized. Additionally, this bond exhibits a strikingly low bond order, with a Wiberg bond order of 0.507. Hyperconjugation between the π-electrons in the C_2N_2 unit and the σ*(P–X) orbital occurs, in turn weakening the P–X bond which is in agreement to similar observations by Gudat.[10] This analysis revealed similar results for **2b**, with the As–Cl bond being heavily polarized. The natural charges being 1.393 and -0.546 for As and Cl respectively and a Wiberg bond order of 0.576.

Subsequently, the corresponding phosphenium and arsenium cations were produced by utilizing a range of chloride abstraction agents; $AlCl_3$, $GaCl_3$ and trimethylsilyl trifluoromethanesulfonate (TMSOTf), giving the cationic complexes **3a–c** and **4a–c** in yields generally above 80%. Single crystals of all of these compounds, suitable for X-ray diffraction, were grown from a saturated CH_2Cl_2 solution cooled to -40 °C (Figure 2 and ESI). All bonding in these structures are as expected and lie within similar ranges of related compounds.[11] With the exception of **4c**, the crystal structures revealed the presence of close contacts between the central pnictogen atom and the counterion. The Pn···Cl distances for **3a–b** (3.4963(9)–3.4967(7) Å) and **4a–b** (3.5677(8)–3.5754(6) Å) are within the van der Waals radii of 3.55 Å and 3.80 Å respectively. This is also the case for **3c** where the P···O interatomic distance of 2.8238(16) Å is well within the combined van der Waals radii of 3.32 Å.

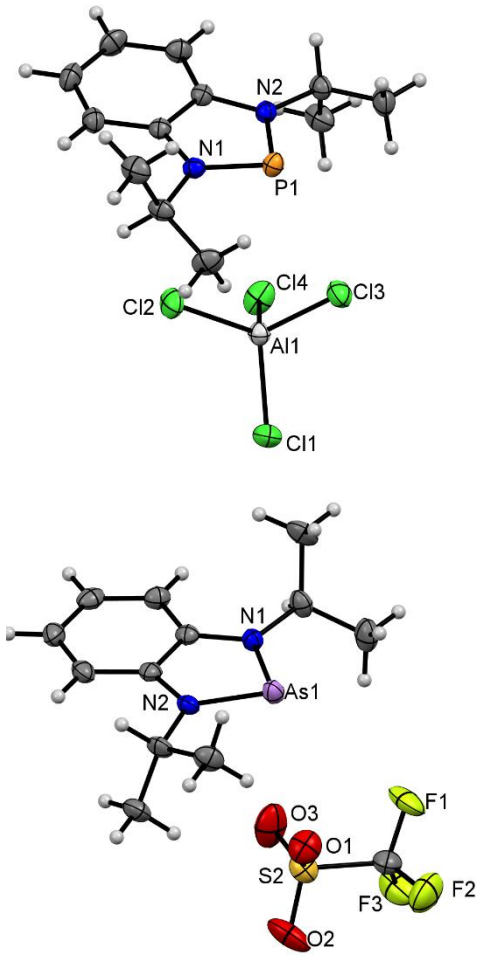

Figure 2. Solid-state structure of **3a** (top) and **4c** (bottom). Thermal ellipsoids drawn at 50% probability.

Table 1. Photophysical properties of phosphole and arsole derivatives.

Compound	Solvent	λ_{abs} / nm (ε / 10^4 M^{-1} cm^{-1})	λ_{max} / nm	τ /ns	ϕ / %
2a	$CHCl_3$	269 (8.3) sh, 280 (4.5) sh	384	1.4 (32%) 8.3 (68%)	0.5
	MeCN	250 (6.1), 287 (1.6) sh	393	1.3 (51%) 5.9 (49%)	0.7
3a	$CHCl_3$	269 (7.0) sh, 280 (5.2) sh, 333 (1.6)	384	1.3 (57%) 5.1 (43%)	0.1
	MeCN	251 (6.5), 325 (1.1)	393	1.5 (50%) 5.7 (50%)	1.7
3b	$CHCl_3$	269 (8.9) sh, 280 (5.7) sh	384	0.9 (45%) 3.7 (55%)	0.3
	MeCN	250 (7.2), 287 (1.6) sh	393	1.4 (51%) 5.9 (49%)	1.4
3c	$CHCl_3$	269 (7.6) sh, 280 (4.9) sh	384	0.8 (33%) 2.8 (67%)	0.2
	MeCN	250 (6.5), 287 (2.7) sh	393	1.3 (49%) 5.0 (51%)	1.7
2b	$CHCl_3$	269 (8.0) sh, 282 (4.3) sh, 332 (1.6)	387	1.6 (39%) 9.9 (61%)	0.09
	MeCN	265 (3.7) sh, 315 (1.4)	393	1.6 (54%) 5.0 (46%)	1.1
4a	$CHCl_3$	269 (8.8) sh, 282 (5.1) sh	384	1.2 (45%) 8.6 (55%)	0.3
	MeCN	247 (5.4) sh, 284 (1.9)	393	1.3 (52%) 5.0 (48%)	0.5
4b	$CHCl_3$	269 (7.9) sh, 282 (4.4) sh, 355 (2.7)	384	1.3 (54%) 8.9 (46%)	0.08
	MeCN	254 (7.3), 310 (1.6)	393	1.6 (49%) 6.1 (51%)	0.7
4c	$CHCl_3$	269 (8.4) sh, 282 (4.5) sh, 341 (2.0)	384	1.1 (34%) 9.5 (66%)	0.1
	MeCN	254 (8.0), 310 (1.8)	393	1.6 (46%) 5.4 (54%)	1.2

Following structural analyses elucidating the counter-ion interaction, we were curious as to whether these compounds exhibited any interesting photophysical properties on account of their coordination sphere about the cationic pnictogen center and their 10π Hückel aromatic nature.[12,13] To date, there have been few attempts to explore the photophysical properties of such compounds and their derivatives.[14] These properties were measured for compounds **2a**–**4c**, which are summarized in Table 1. The UV-vis absorption spectra were obtained from degassed solutions (acetonitrile and chloroform) of the compounds revealing changes in spectral appearance and band positioning depending on both the cationic heteroatom center and the counter-ion (Figure 3). For example, the absorption spectra of the arsole derivative in chloroform (Figure 3, top left) revealed a single peak, centered at 355 nm in the case of **4b** (thus accounting for the pale color of the compound). This variance in wavelength and intensity suggests some degree of cation-anion aggregation in solution, with the $GaCl_4$ anion being the most pronounced example. For the phosphole derivative in chloroform (Figure 3, top right), only **3a** exhibited a discrete peak between 300 nm and 400 nm, centered at 333 nm. Interestingly, it was found that the spectra in a more polar acetonitrile solution were hypsochromically shifted with respect to the chloroform solutions (Figure 3, bottom left and right). Indeed, the lowest energy bands of **4b** and **4c** exhibit a shift from 355 nm and 341 nm, respectively, to 310 nm. In all cases these absorption bands are ascribed to $^1\pi \rightarrow \pi^*$ transitions, supported by TD-DFT calculations (see ESI) which suggest that the lowest energy transitions arise from π and π* orbitals. The blue shift observed in acetonitrile may be due to the inherent (ground state) dipole moment caused by the P^+/As^+ center. This was further evidenced by DFT calculations which suggest that the counterions are weakly associated with the positive centers (see ESI).

The arsole and phosphole derivatives were shown to be emissive following irradiation (λ_{exc} = 330 nm) of the lowest energy absorption bands (Figure 4). Measurements were obtained in degassed acetonitrile and chloroform solutions and are generally similar, exhibiting broad bands with some vibrational features centered at 393 nm and 384 nm, respectively. Quantum yields were obtained and typically in the range of 0.1-2%. Interestingly, an observed increase in quantum yield was noted for all compounds in acetonitrile solution compared with chloroform. Time-resolved measurements (λ_{exc} = 295 nm) produced profiles that fit best to a biexponential decay giving a short lifetime component on the order of 1 ns, and a second longer component ranging from 2.8 ns for **3c** in chloroform to 9.9 ns for **2b** in chloroform.

The observed data, in the case of the phosphole derivatives, suggests a variation in lifetime as a function of the counterion, although it was noted that in general the longer components of the decays were shorter than their arsole counterparts. In all cases the short lifetimes were consistent with a fluorescence process. The luminescence lifetimes of the arsole derivatives also follow a trend between solvents, as the longer component decreases in acetonitrile with respect to chloroform. For example, for **2b** this component decreased from 9.0 ns in chloroform to 5.0 ns in acetonitrile. Due to the relatively small Stokes shift of the emission, short lifetimes and small shift (9 nm) in emission maxima between the two solvents, the emissive state of these species is ascribed to a dominant $^1\pi \rightarrow \pi^*$ character.

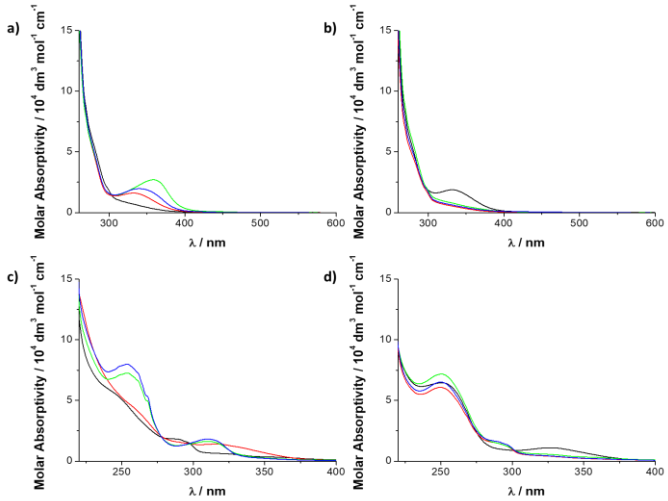

Figure 3. UV-Visible absorption spectra of arsole and phosphole derivatives in chloroform (a and b respectively) and acetonitrile (c and d respectively). Counterions are Cl^- (red), $AlCl_4^-$ (black), $GaCl_4^-$ (green) and OTf^- (blue).

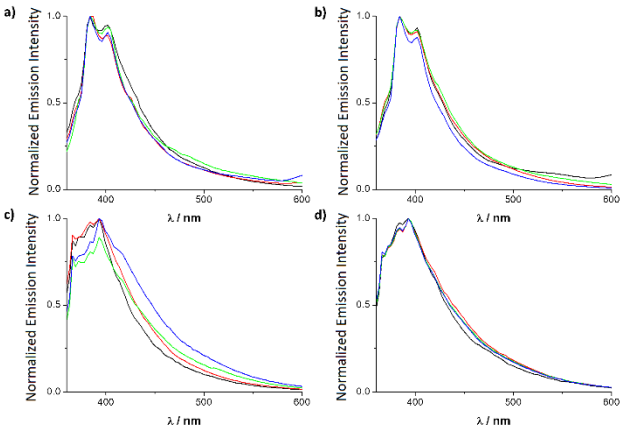

Figure 4. Steady-state emission spectra of arsole and phosphole derivatives in chloroform (a and b respectively) and acetonitrile (c and d respectively). Counterions are Cl^- (red), $AlCl_4^-$ (black), $GaCl_4^-$ (green) and OTf^- (blue). λ_{exc} = 330 nm, C = 10^{-5} M.

Further to phosphenium generation, reduction of the starting phosphole was undertaken to form a dimeric species *via* a one-electron reduction of **2a** using Mg turnings to give the product **5**, which contained a central P–P bond (Figure 5). Single crystals were grown from a saturated solution of CH_2Cl_2 cooled to -40 °C with metrics commensurate with similar structures (2.2379(6) *vs.* 2.2406(6)–2.3012(7)).[15] In addition, the crystal structure revealed an anti-conformation of the two fused heterocyclic rings about the central P–P bond, which is presumed to be a result of minimizing steric repulsion between the isopropyl groups as evidenced by the inequivalence of the methyl groups in the ^{1}H NMR spectrum.

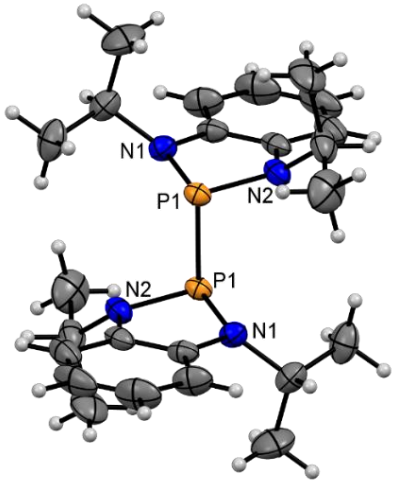

Figure 5. Solid-state structure of **5**. Thermal ellipsoids drawn at 50% probability.

Given the possibility for the P–P bond in **5** to break homolytically and form a radical species, EPR studies were undertaken. Complex **5** was found to be EPR silent in the solid-state, even when heated to 350 K. Dissolving **5** in toluene and performing solution-state EPR at ambient temperature also failed to produce an EPR signal. However, the EPR spectrum of a toluene solution of **5** recorded at 350 K shows a well-defined doublet signal, centered at g_{iso} = 2.0025 (Figure 6). The observed a_{iso} = 130 MHz hyperfine coupling arises from coupling of the unpaired electron to one ^{31}P nucleus, and is consistent with previous reports of structurally similar radicals formed upon P–P bond cleavage of $[(CH)_2(NR)_2P]_2$ dimers.[6] Although no further hyperfine coupling could be resolved (even using an experimental modulation amplitude of 0.5 G), inclusion of two equivalent ^{14}N nuclei with a_{iso} = 10 MHz resulted in an improved fit to the experimental line-shape. Furthermore, DFT calculations of the radical species were performed using the ORCA package (see ESI for details). Spin-orbit coupling effects were accounted for using a mean-field (SOMF(1X)) approach which predicted an a_{iso} of 113.7 MHz from P and 8.6 MHz from N, which are in good agreement with experimental data. DFT also supports the localization of the electron mainly on phosphorus atom, with spin charges of 0.67 e on P, and 0.11 e on each N lying in *p*-orbitals perpendicular to the N–P–N plane (Figure 7).

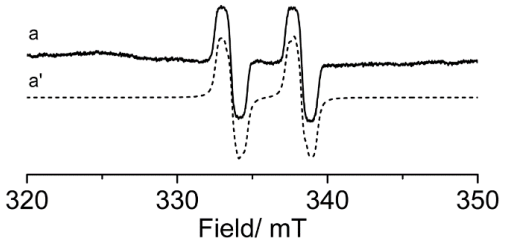

Figure 6. Continuous-wave EPR spectrum recorded at 350 K of a toluene solution of (a) **5**. Corresponding simulation are shown in a′.

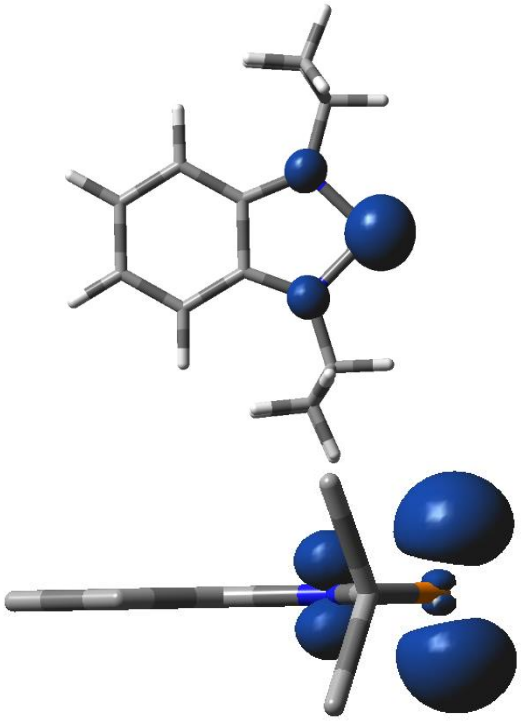

Figure 7. Theoretical spin density plots of radical formed from **5**.

Upon attempting to synthesize the arsenic dimer congener using the analogous method for the formation of **5**, single crystals were formed from a saturated CH_2Cl_2 solution, suitable for X-ray diffraction. Structural analyses revealed that as opposed to dimer formation, the arsole 2-iodo-1,3-diisopropyl-benzodiazarsole (**6**) had instead been formed which was supported by NMR spectroscopic analyses which showed magnetically equivalent methyl groups of the ^{i}Pr moieties similar to **2a**–**b**. It is possible that the arsenic dimer is formed using this methodology however, the introduction of iodine to initiate the reduction reaction then oxidatively adds across the dimer to garner **6** (Scheme 1, Figure 8).

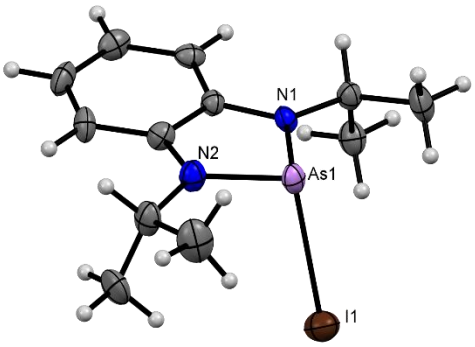

Figure 8. Solid-state structure of **6**. Thermal ellipsoids drawn at 50% probability.

CONCLUSIONS

Through judicial application of a plethora of spectroscopic techniques coupled with computational modelling, this work has probed electronic effects of exchanging counterion of various pnictenium salts. This outlines how slight electronic perturbations are witnessed in the π to π* transitions in the absorbance and luminescence spectra due to electrostatic effects on the cationic heterocycle. Finally, EPR has shown how thermally induced homolytic bond cleavage of diphosphines is possible with these systems, with accompanying theoretical studies confirming predominantly phosphorus-based spin density.

EXPERIMENTAL SECTION

General experimental.

All reactions were carried out under an atmosphere of dinitrogen using standard Schlenk and glove box techniques. With the exception of THF, all solvents used were dried by passing through an alumina column incorporated into an MB SPS-800 solvent purification system, degassed and finally stored in an ampoule fitted with a Teflon valve under a dinitrogen atmosphere. THF was dried over molten potassium for three days and distilled over argon. Deuterated solvents were distilled and/or dried over molecular sieves and stored in a glove box before use. Starting materials were purchased from commercial suppliers and used as received. ^{1}H, ^{13}C{^{1}H}, ^{19}F, ^{27}Al, ^{31}P and ^{31}P{^{1}H} NMR spectra were recorded on a Bruker Avance 300, 400 or 500 MHz spectrometer. Chemical shifts are expressed as parts per million (ppm, δ) and are referenced to $CDCl_3$ (7.26/77.16 ppm), C_6D_6 (7.16/128.06 ppm) or C_6D_5Br (7.28/122.4 ppm for the most downfield resonance) as internal standards. Multinuclear NMR spectra were referenced to H_3PO_4 (^{31}P), $CFCl_3$ (^{19}F) and $Al(NO_2)_3$ (^{27}Al). The description of signals includes s = singlet, d = doublet, t = triplet, q = quartet, sept = septet and m = multiplet. All coupling constants are absolute values and are expressed in Hertz (Hz). IR-Spectra were measured on a Shimadzu IR Affinity-1 photospectrometer. The description of signals includes s = strong, m = medium, w = weak, sh = sharp and br = broad. Mass spectra were measured on a Waters LCT Premier/XE or a Waters GCT Premier spectrometer.

Synthesis of reagents and products.

1: A round bottomed flask equipped with a magnetic stirrer bar was charged with *ortho*-phenylenediamine (2.0 g, 18.5 mmol, 1 equiv.), potassium carbonate (5.1 g, 37.0 mmol, 2 equiv.) and excess 2-iodopropane (20.4 g, 120.0 mmol, 6.5 equiv.). The solution was heated to reflux for two hours, after which time the solution was cooled to ambient temperature. Hexane (30 mL) was subsequently added and the mixture was washed with water (50 mL). The product was extracted from the aqueous phase using hexane (3 x 20 mL), combining the organic phases after each extraction. The solution was dried using anhydrous magnesium sulfate and the solvent was removed under reduced pressure to afford a viscous dark brown oil. Subsequently the oil was passed through a silica plug (0.2 cm, toluene) and the solvent was again removed under reduced pressure to give a red/brown

oil. The resulting oil was purified further using a Kugelröhr short path distillation (180 °C, 5 mbar) to yield a colorless oil. Yield: 2.9 g, 15.1 mmol, 80%. **^{1}H NMR** (500 MHz, $CDCl_3$, 295 K) δ/ppm: 6.87–6.85 (m, 2H, Ar–H), 6.80–6.76 (m, 2H, Ar–H), 3.65 (sept, $^3J_{HH}$ = 6.3 Hz, 2H, C<u>H</u>$(CH_3)_2$), 3.23 (br. s, 2H, NH), 1.32 (d, $^3J_{HH}$ = 6.3, 12H, CH(C<u>H</u>$_3)_2$). **^{13}C{^{1}H} NMR** (126 MHz, $CDCl_3$, 295 K) δ/ppm: 136.8 (2C, Ar), 118.9 (2C, Ar), 113.2 (2C, Ar), 44.4 (2C, <u>C</u>H$(CH_3)_2$, 23.3 (4C, CH(<u>C</u>H$_3)_2$). **IR** ν_{max} (cm^{-1}): 2962 (m), 1599 (m), 1506 (m), 1253 (m), 1177 (m), 741 (m), 399 (s, sh). **HRMS** (EI^+) *m/z* calculated for $[M]^+$ $[C_{12}H_{20}N_2]^+$: 192.1626, found: 192.1624.

2a: A three-necked flask was fitted with a magnetic stirrer bar and charged with compound **1** (1.50 g, 7.8 mmol, 1 equiv.) in toluene (10 mL) and phosphorus trichloride (0.82 mL, 9.4 mmol, 1.2 equiv.). The solution was cooled to 0 ˚C and triethylamine (2.61 mL, 18.7 mmol, 2.4 equiv.) was added dropwise whilst stirring. The reaction was warmed to ambient temperature and stirred for 24 hours. Using a filter cannula, the solution was transferred to a Schlenk tube and the solvent was removed *in vacuo*. The precipitate was washed with pentane (3 x 5 mL) to yield the product as a white solid. Single crystals suitable for X-ray diffraction were grown from a concentrated solution of CH_2Cl_2 with a few drops of pentane and cooled to -40 °C. M.p. 95–98 °C. Yield: 1.68 g, 6.54 mmol, 84%. **^{1}H NMR** (500 MHz, $CDCl_3$, 295 K) δ/ppm: 7.08 (s, 4H, Ar–H), 4.32 (sept, $^3J_{HH}$ = 6.6 Hz, 2H, C<u>H</u>$(CH_3)_2$), 1.69 (d, $^3J_{HH}$ = 6.6 Hz, 12H, CH(C<u>H</u>$_3)_2$). **^{13}C{^{1}H} NMR** (126 MHz, $CDCl_3$, 295 K) δ/ppm: 136.8 (2C, Ar), 121.3 (2C, Ar), 111.6 (2C, Ar), 48.0 (2C, <u>C</u>H$(CH_3)_2$), 22.3 (4C, CH(<u>C</u>H$_3)_2$). **^{31}P{^{1}H} NMR** (202 MHz, $CDCl_3$, 295 K) δ/ppm: 147.2 (s). **IR** ν_{max} (cm^{-1}): 2978 (w), 1487 (m), 1371 (w), 1260 (m), 1159 (m), 930 (m), 741 (s), 492 (m). **HRMS** (EI^+) *m/z* calculated for $[M]^+$ $[C_{12}H_{18}PN_2Cl]^+$: 256.0896, found: 256.0901.

2b: A three-necked flask was fitted with a magnetic stirrer bar and charged with compound **1** (1.17 g, 6.07 mmol, 1 equiv.) in toluene (10 mL) and arsenic trichloride (1.32 g, 7.3 mmol, 1.2 equiv.). The solution was cooled to 0 °C and triethylamine (2.03 mL, 14.6 mmol, 2.4 equiv.) was added dropwise whilst stirring. The reaction was warmed to ambient temperature before being stirred for 24 hours. Using a filter cannula, the solution was transferred to a Schlenk tube and the solvent was removed *in vacuo*. The precipitate was washed with pentane (3 x 5 mL) to yield the product as a white solid. M.p. 96–99 °C. Yield: 1.51 g, 5.02 mmol, 83%. Single crystals suitable for X-ray diffraction were grown from a concentrated solution of CH_2Cl_2 with a few drops of pentane and cooled to -40 °C. **^{1}H NMR** (500 MHz, $CDCl_3$, 295 K) δ/ppm: 7.04 (s, 4H, Ar–H), 4.46 (sept, $^3J_{HH}$ = 6.5 Hz, 2H, C<u>H</u>$(CH_3)_2$), 1.70 (d, $^3J_{HH}$ = 6.5 Hz, 12H, CH(C<u>H</u>$_3)_2$). **^{13}C{^{1}H} NMR** (126 MHz, $CDCl_3$, 295 K) δ/ppm: 139.0 (2C, Ar), 120.7 (2C, Ar), 111.8 (2C, Ar), 49.1 (2C, <u>C</u>H$(CH_3)_2$, 23.4 (4C, CH(<u>C</u>H$_3)_2$). **IR** ν_{max} (cm^{-1}): 2974 (w), 1477 (m), 1388 (m), 1292 (s, sh), 1153 (m), 998 (m), 891 (m), 745 (m), 550 (m), 473 (m). **HRMS** (ES^+) *m/z* calculated for $[M]^+$ $[C_{12}H_{18}AsN_2Cl]^+$: 300.0374, found: 300.0376.

General procedure 1: Compound **2a** (100 mg, 0.39 mmol, 1 equiv.) or **2b** (100 mg, 0.33 mmol, 1 equiv.) was dissolved in CH_2Cl_2 (2 mL) and added to a stirring solution of the halide abstracting reagent (1 equiv.) in CH_2Cl_2 (2 mL). The red/orange solution was stirred for 2 hours at ambient temperature, after which the solvent was removed *in vacuo* to afford a red/yellow solid. The solid was washed with pentane (3 x 2 mL and further dried *in vacuo* to afford the product **3a–4c**. Single crystals suitable for X-ray diffraction were grown from a concentrated solution of CH_2Cl_2 with a few drops of pentane and cooled to -40 °C.

3a: Compound **3a** was synthesized according to general procedure 1 using **2a** (100 mg, 0.39 mmol, 1 equiv.) and $AlCl_3$ (52 mg, 0.39 mmol, 1 equiv.). M.p. 101–104 °C. Yield: 121 mg, 0.31 mmol, 80%. **^{1}H NMR** (500 MHz, C_6D_5Br, 295 K) δ/ppm: 7.30 (br. m, 2H, Ar–H), 7.22 (br. m, 2H, Ar–H), 4.45 (sept, $^3J_{HH}$ = 6.2 Hz, 2H, C<u>H</u>$(CH_3)_2$), 1.50 (d, $^3J_{HH}$ = 6.2 Hz, 12H, CH(C<u>H</u>$_3)_2$). **^{13}C{^{1}H} NMR** (126 MHz, C_6D_5Br, 295 K) δ/ppm: 129.8 (2C, Ar), 118.8 (2C, Ar), 105.4 (2C, Ar), 43.7 (2C, <u>C</u>H$(CH_3)_2$, 15.0 (4C, CH(<u>C</u>H$_3)_2$). **^{31}P{^{1}H} NMR** (202 MHz, C_6D_5Br, 295 K) δ/ppm: 207.7 (s). **^{27}Al NMR** (130 MHz, C_6D_5Br, 295 K) δ/ppm: 103.8 (s). **IR** ν_{max} (cm^{-1}): 2982 (m), 1585 (w), 1466 (m), 1393 (m), 1153 (m), 1008 (w), 930 (w), 748 (s, sh), 496 (m). **HRMS** (EI^+) *m/z* calculated for $[M^+]$ $[C_{12}H_{18}N_2P]^+$: 221.1208, found 221.1209.

3b: Compound **3b** was synthesized according to general procedure 1 using **2a** (100 mg, 0.39 mmol, 1 equiv.) and $GaCl_3$ (69 mg, 0.39 mmol, 1 equiv.). M.p. 96–99 °C. Yield: 143 mg, 0.33 mmol, 85%. **^{1}H NMR** (500 MHz, C_6D_5Br, 295 K) δ/ppm: 7.34 (br. m, 2H, Ar–H), 7.24 (br. m, 2H, Ar–H), 4.49 (sept, $^3J_{HH}$ = 6.3 Hz, 2H, C<u>H</u>$(CH_3)_2$), 1.51 (d, $^3J_{HH}$ = 6.3 Hz, 12H, CH(C<u>H</u>$_3)_2$). **^{13}C{^{1}H} NMR** (126 MHz, C_6D_5Br, 295 K) δ/ppm: 129.9 (2C, Ar), 119.3 (2C, Ar), 105.6 (2C, Ar), 44.0 (2C, <u>C</u>H$(CH_3)_2$, 15.2 (4C, CH(<u>C</u>H$_3)_2$). **^{31}P{^{1}H} NMR** (202 MHz, C_6D_5Br, 295 K) δ/ppm: 212.9 (s). **IR** ν_{max} (cm^{-1}): 2985 (w), 1566 (w), 1472(w), 1395 (w), 1346 (w), 1153 (m), 1115 (m), 989 (m), 746 (s, sh). **HRMS** (EI^+) *m/z* calculated for $[M^+]$ $[C_{12}H_{18}N_2P]^+$: 221.1208, found 221.1205.

3c: Compound **3c** was synthesized according to general procedure 1 using **2a** (100 mg, 0.39 mmol, 1 equiv.) and TMSOTf (104 mg, 0.47 mmol, 1.2 equiv.). M.p. 108–112 °C. Yield: 92 mg, 0.25 mmol, 64%. **^{1}H NMR** (500 MHz, $CDCl_3$, 295 K) δ/ppm: 7.70 (br. m, 2H, Ar–H), 7.61 (br. m, 2H, Ar–H), 4.97 (sept, $^3J_{HH}$ = 6.3 Hz, 2H, C<u>H</u>$(CH_3)_2$), 1.87 (d, $^3J_{HH}$ = 6.3 Hz, 12H, CH(C<u>H</u>$_3)_2$). **^{13}C{^{1}H} NMR** (126 MHz, $CDCl_3$, 295 K) δ/ppm: 138.6 (2C, Ar), 127.2 (2C, Ar), 114.3 (2C, Ar), 52.5 (2C, <u>C</u>H$(CH_3)_2$, 23.8 (4C, CH(<u>C</u>H$_3)_2$). **^{31}P{^{1}H} NMR** (202 MHz, $CDCl_3$, 295 K) δ/ppm: 216.5 (s). **^{19}F NMR** (471 MHz, $CDCl_3$, 295 K) δ/ppm: -78.4 (s, 3F, $O_3SCF_3^-$). **IR** ν_{max} (cm^{-1}): 2992 (w), 1474 (w), 1395 (w), 1377 (w), 1246 (s), 1151 (s), 1022 (s), 754 (s), 627 (s), 571 (s), 513 (s), 496 (s), 417 (m). **HRMS** (EI^+) *m/z* calculated for $[M^+]$ $[C_{12}H_{18}N_2P]^+$: 221.1208, found 221.1207.

4a: Compound **4a** was synthesized according to general procedure 1 using **2b** (100 mg, 0.33 mmol, 1 equiv.) and $AlCl_3$ (44 mg, 0.33 mmol, 1 equiv.). M.p. 105–109 °C. Yield: 124 mg, 0.29 mmol, 87%. **^{1}H NMR** (500 MHz, C_6D_5Br, 295 K) δ/ppm: 7.19 (br. m, 2H, Ar–H), 7.04 (br. m, 2H, Ar–H), 4.43 (br. m, 2H, C<u>H</u>$(CH_3)_2$), 1.49 (d, $^3J_{HH}$ = 6.2 Hz, 12H, CH(C<u>H</u>$_3)_2$). **^{13}C{^{1}H} NMR** (126 MHz, C_6D_5Br, 295 K) δ/ppm: 132.4 (2C, Ar), 117.1 (2C, Ar), 105.0 (2C, Ar), 43.8 (2C, <u>C</u>H$(CH_3)_2$, 15.9 (4C, CH(<u>C</u>H$_3)_2$). **^{27}Al NMR** (130 MHz, C_6D_5Br, 295 K) δ/ppm: 104.5 (s). **IR** ν_{max} (cm^{-1}): 2992 (w), 1568 (w), 1393 (w), 1172 (w), 1153 (w), 989 (w), 746 (m), 467 (s, br). **HRMS** (ES^+) *m/z* calculated for $[M]^+$ $[C_{12}H_{18}AsN_2]^+$: 265.0686, found: 265.0692.

4b: Compound **4b** was synthesized according to general procedure 1 using **2b** (100 mg, 0.33 mmol, 1 equiv.) and $GaCl_3$ (58 mg, 0.33 mmol, 1 equiv.). M.p. 80–82 °C. Yield: 132 mg, 0.28 mmol, 84%. **^{1}H NMR** (500 MHz, C_6D_5Br, 295 K)

δ/ppm: 7.26 (m, 2H, Ar–H), 7.11 (m, 2H, Ar–H), 4.54 (sept, $^3J_{HH}$ = 6.3 Hz, 2H, C<u>H</u>(CH$_3$)$_2$), 1.51 (d, $^3J_{HH}$ = 6.3 Hz, 12H, CH(C<u>H</u>$_3$)$_2$). **^{13}C{^{1}H} NMR** (126 MHz, C_6D_5Br, 295 K) δ/ppm: 133.1 (2C, Ar), 118.7 (2C, Ar), 105.7 (2C, Ar), 45.0 (2C, <u>C</u>H(CH$_3$)$_2$, 16.4 (4C, CH(<u>C</u>H$_3$)$_2$). **IR** ν_{max} (cm^{-1}): 2980 (m), 1566 (w), 1462 (w), 1393 (w), 1375 (w), 1269 (w), 1153 (m), 949 (w, br), 746 (m). **HRMS** (ES$^+$) *m/z* calculated for [M]$^+$ [$C_{12}H_{18}AsN_2$]$^+$: 265.0686, found: 265.0692; *m/z* calculated for [M]$^-$ [$GaCl_4$]$^-$: 208.8010, found: 208.8014.

4c: Compound **4c** was synthesized according to general procedure 1 using **2b** (100 mg, 0.33 mmol, 1 equiv.) and TMSOTf (88 mg, 0.40 mmol, 1.2 equiv.). M.p. 118–121 °C. Yield: 112 mg, 0.27 mmol, 82%. **^{1}H NMR** (500 MHz, $CDCl_3$, 295 K) δ/ppm: 7.59 (br. m, 2H, Ar–H), 7.53 (br. m, 2H, Ar–H), 5.06 (sept, $^3J_{HH}$ = 6.2 Hz, 2H, C<u>H</u>(CH$_3$)$_2$), 1.90 (d, $^3J_{HH}$ = 6.2 Hz, 12 H, CH(C<u>H</u>$_3$)$_2$). **^{13}C{^{1}H} NMR** (126 MHz, $CDCl_3$, 295 K) δ/ppm: 141.4 (2C, Ar), 126.4 (2C, Ar), 114.3 (2C, Ar), 53.4 (2C, <u>C</u>H(CH$_3$)$_2$, 24.8 (4C, CH(<u>C</u>H$_3$)$_2$). **^{19}F NMR** (471 MHz, $CDCl_3$, 295 K) δ/ppm: -78.1 (s, 3F, $O_3SCF_3^-$) **IR** ν_{max} (cm^{-1}): 2988 (w), 1466 (w), 1393 (w), 1248 (s), 1144 (s), 1024 (s), 766 (m), 633 (s), 571 (m) and 515 (m). **HRMS** (ES$^+$) *m/z* calculated for [M]$^+$ [$C_{12}H_{18}AsN_2$]$^+$: 265.0686, found: 265.0689; *m/z* calculated for [M]$^-$ [CF_3O_3S]$^-$: 148.9520, found: 148.9524.

5: Compound **2a** (300 mg, 1.17 mmol, 1 equiv.) was dissolved in THF (5 mL). Magnesium turnings (43 mg, 1.76 mmol. 1.5 equiv.) and a crystal of iodine were added to the solution, which was left to stir for 24 hours. The orange solution was filtered through celite and the solvent removed *in vacuo.* Single crystals suitable for X-ray diffraction were grown from a concentrated solution of CH_2Cl_2 with a few drops of pentane and cooled to -40 °C. M.p. 142–146 °C. Yield: 404 mg, 0.91 mmol, 78%. **^{1}H NMR** (400 MHz, C_6D_6, 295 K) δ/ppm: 6.98–6.96 (m, 4H, Ar–H), 6.74–6.72 (m, 4H, Ar–H), 3.63 (sept, $^3J_{HH}$ = 6.5 Hz, 4H, C<u>H</u>(CH$_3$)$_2$), 1.44 (d, $^3J_{HH}$ = 6.5 Hz, 12H, CH(C<u>H</u>$_3$)$_2$) and 1.05 (d, $^3J_{HH}$ = 6.5 Hz, 12H, CH(C<u>H</u>$_3$)$_2$). **^{13}C{^{1}H} NMR** (101 MHz, C_6D_6, 295 K) δ/ppm: 144.7 (4C, Ar), 120.3 (4C, Ar), 113.3 (4C, Ar), 50.2 (4C, <u>C</u>H(CH$_3$)$_2$), 23.8 (4C, CH(<u>C</u>H$_3$)$_2$), 21.4 (4C, CH(<u>C</u>H$_3$)$_2$). **^{31}P{^{1}H} NMR** (162 MHz, C_6D_6, 295 K) δ/ppm: 87.2 (s). **IR** ν_{max} (cm^{-1}): 2978 (m), 1471 (m), 1377 (m), 1248 (m), 1157 (m, br), 1028 (w), 878 (m), 731 (m), 634 (m) and 544 (m). **HRMS** (EI$^+$) *m/z* calculated for [M]$^+$ [$C_{12}H_{18}N_2P$]$^+$: 221.1208, found: 221.1211.

6: Compound **2b** (41 mg, 0.14 mmol, 1 equiv.) was dissolved in THF (5 mL). Magnesium turnings (5 mg, 0.21 mmol, 1.5 equiv.) and a crystal of iodine were added to the solution, which was left to stir for 24 hours. The solvent was removed *in vacuo* and CH_2Cl_2 (5 mL) was added. The solution was filtered through Celite twice and the solvent was again removed *in vacuo* to afford the pure product. Single crystals suitable for X-ray diffraction were grown from a concentrated solution of CH_2Cl_2 with a few drops of pentane and cooled to -40 °C. M.p. 114–116 °C. Yield: 33 mg, 0.08 mmol, 60%. **^{1}H NMR** (500 MHz, $CDCl_3$, 295 K) δ/ppm: 7.12 (s, 4H, Ar–H), 4.58 (sept, $^3J_{HH}$ = 5.9 Hz, 2H, C<u>H</u>(CH$_3$)$_2$), 1.74 (d, $^3J_{HH}$ = 5.9 Hz, 12H, CH(C<u>H</u>$_3$)$_2$). **^{13}C{^{1}H} NMR** (126 MHz, $CDCl_3$, 295 K) δ/ppm: 139.6 (2C, Ar), 121.6 (2C, Ar), 112.5 (2C, Ar), 50.0 (2C, <u>C</u>H(CH$_3$)$_2$) and 22.2 (4C, CH(<u>C</u>H$_3$)$_2$). **IR** ν_{max} (cm^{-1}): 2970 (w), 1473 (m), 1389 (m), 1294 (m), 1260 (m), 1153 (m), 1018 (w), 995 (w), 889(w), 739 (m) and 552 (w). **HRMS** (ES$^+$) *m/z* calculated for [M]$^+$ [$C_{12}H_{18}AsN_2$]$^+$: 265.0686, found: 265.0675.

Photophysical studies

UV-Vis studies were performed on a Shimadzu UV-1800 spectrophotometer as deaerated chloroform or acetonitrile solutions (1×10^{-5} M) as stated. Photophysical data were obtained on a JobinYvon–Horiba Fluorolog spectrometer fitted with a JY TBX picosecond photodetection module as chloroform or acetonitrile solutions as stated. Emission spectra were uncorrected and excitation spectra were instrument corrected. The pulsed source was a Nano-LED configured for 295 nm output operating at 1 MHz. Luminescence lifetime profiles were obtained using the JobinYvon–Horiba FluoroHub single photon counting module and the data fits yielded the lifetime values using the provided DAS6 deconvolution software. Quantum yield measurements were obtained on aerated solutions of the compounds using anthracene in deaerated ethanol as a standard (Φ = 0.27).[16]

EPR studies

The continuous wave (CW) X-band EPR measurements were performed on a Bruker EMX spectrometer utilizing an ER4119HS resonator, using 100 kHz field modulation, 1.0 mW microwave power and < 1 G modulation amplitude, at 298 or 350 K. Simulations of the EPR spectra were performed using the Easyspin software package running within the MathWorks® MatLab® environment.[17]

Theoretical studies

DFT calculations were performed using the graphical interface WebMO computational platform, which employed the Gaussian 09 package.[18] For the phosphorus containing compounds the structures used were initially geometry optimized using the hybrid functional Becke, three-parameter, Lee-Yang-Parr (B3LYP)[19] and the Pople split valence basis set 6-31+G(2d,p) on all atoms.[20] Natural bond orbital (NBO) analysis was then performed on the phosphole **2a** and phosphenium cation. The arsenic containing species were optimized using B3LYP and a split basis set. The arsenic atom was treated with B3LYP and the effective core potential Los Alamos National Laboratory 2-double-z (LANL2DZ),[21] whilst all other atoms again used B3LYP/6-31+G(2d,p). NBO analysis was subsequently performed on the arsole **2b** and arsenium cation.

For theoretical photophysical studies, geometry optimized structures with no solvent effects were again optimized using a polarizable continuum model (PCM) to model solvent effects. The resulting lowest energy structures were then used to calculate excited state transitions using TD-DFT methods. The basis set and functional cam-B3LYP/6-31+G(2d,p) were employed and in addition an UltraFine integration grid was used.[22] Molecular orbital and natural bond orbital (NBO) calculations were additionally performed on the solvent optimized structures. Molecular orbital images were visualized using the Avogadro package.[23]

For theoretical EPR studies, geometry optimization of the $C_6H_4N_2(^iPr)_2P\cdot$ radical was performed using the Perdew–Burke-Ernzerhof UPBE0 hybrid functional[22] and Pople split valence basis set 6-31+G(2d,p)[20] on the graphical interface WebMO computational platform, which employed the Gaussian 09 package.[18] EPR simulations and spin charge density DFT calculations were performed in the ORCA package v4.0[25] and used the PBE0 functional with def2-TZVP basis set on all atoms.[26] Spin-orbit coupling effects were accounted for using a mean field (SOMF(1X)) approach.[27]

ASSOCIATED CONTENT

Supporting Information.
The Supporting Information is available free of charge on the ACS Publications website.

AUTHOR INFORMATION

Corresponding Author

E-mail for R.L.M.: MelenR@cardiff.ac.uk

Notes

The authors declare no competing financial interests.

ACKNOWLEDGMENT

We would like to acknowledge Ben D. Ward for his assistance with computational modelling, and Andrea Folli for useful discussions.

Author Contributions

The manuscript was written through contributions of all authors. All authors have given approval to the final version of the manuscript.

Funding Sources

S. J. A. Pope would like to thank the Leverhulme Trust for financial support (RPG-2015-359).

REFERENCES

(1) a) Dimroth, K.; Hoffmann, P., *Angew. Chem. Int. Ed.* **1964**, *3*, 384-384; b) Payrastre, C.; Madaule, Y.; Wolf, J. G.; Kim, T. C.; Mazières, M.-R.; Wolf, R.; Sanchez, M., *Heteroat. Chem* **1992**, *3*, 157–162.

(2) Caputo, C. A.; Price, J. T.; Jennings, M. C.; McDonald, R.; Jones, N. D., *Dalton Trans.* **2008**, 3461–3469.

(3) a) Caputo, C. A.; Jennings, M. C.; Tuononen, H. M.; Jones, N. D., *Organometallics* **2009**, *28*, 990–1000; b) Bezpalko, M. W.; Poitras, A. M.; Foxman, B. M.; Thomas, C. M., *Inorg. Chem.* **2017**, *56*, 503–510.

(4) a) Burford, N.; Parks, T. M.; Bakshi, P. K.; Cameron, T. S., *Angew. Chem. Int. Ed.* **1994**, *33*, 1267–1268; b) Burford, N.; Ragogna, P. J.; Sharp, K.; McDonald, R.; Ferguson, M. J., *Inorg. Chem.* **2005**, *44*, 9453–9460; c) Reeske, G.; Hoberg, C. R.; Hill, N. J.; Cowley, A. H., *J. Am. Chem. Soc.* **2006**, *128*, 2800–2801; d) Reeske, G.; Cowley, A. H., *Chem. Commun.* **2006**, 1784–1786.

(5) a) Ayant, Y.; Kernevez, N.; Thevand, A.; Werbelow, L. G.; Culcasi, M.; Gronchi, G.; Tordo, P., *J. Magn. Reson.* **1986**, *70*, 446–451; b) Giffin, N. A.; Hendsbee, A. D.; Roemmele, T. L.; Lumsden, M. D.; Pye, C. C.; Masuda, J. D., *Inorg. Chem.* **2012**, *51*, 11837–11850; c) Puntigam, O.; Förster, D.; Giffin, N. A.; Burck, S.; Bender, J.; Ehret, F.; Hendsbee, A. D.; Nieger, M.; Masuda, J. D.; Gudat, D., *Eur. J. Inorg. Chem.*, **2013**, 2041–2050; d) Giffin, N. A.; Hendsbee, A. D.; Masuda, J. D., *Dalton Trans.* **2016**, *45*, 12636–12638.

(6) Edge, R.; Less, R. J.; McInnes, E. J. L.; Muther, K.; Naseri, V.; Rawson, J. M.; Wright, D. S., *Chem. Commun.* **2009**, 1691–1693.

(7) a) Burck, S.; Gudat, D.; Nättinen, K.; Nieger, M.; Niemeyer, M.; Schmid, D.; *Eur. J. Inorg. Chem.*, **2007**, 5112—5119. b) Schmid, D.; Bubrin, D.; Förster, D.; Nieger, M.; Roeben, E.; Strobel, S.; Gudat, D.; *C. R. Chimie*, **2010**, 13, 998—1005. c) Gans-Eichler, T., Gudat, D., Nieger, M.; *Heteroat. Chem.*, **2005**, 16, 327—338. d) Brazeau, A. L.; Jones, N. D.; Ragogna, P. J.; *Dalton Trans*., **2012**, 41, 7890–7896.

(8) Bond Energies, *Encyclopedia of Inorganic Chemistry*, **2006**, doi: 10.1002/0470862106.id098.

(9) a) Thompson, R. S.; Guler, L. P.; Nelson, E. D.; Yu, Y.-Q.; Kenttämaa, H. I., *J. Org. Chem.* **2002**, *67*, 5076–5084; b) Dordevic, N.; Ganguly, R.; Petkovic, M.; Vidovic, D., *Chem. Commun.* **2016**, *52*, 9789–9792.

(10) Gudat, D.; Haghverdi, A.; Hupfer, H.; Nieger, M., *Chem. Eur. J.* **2000**, *6*, 3414–3425.

(11) see CSD codes: BAYQUP, VADLIX, VADLAP.

(12) Delocalization of the π system in the HOMO of the phosphenium cation can be seen in Fig. S4.5.2 in the supporting information.

(13) Denk, M. K.; Gupta, S.; Lough, A. J., *Eur. J. Inorg. Chem.*, **1999**, 41—49.

(14) a) He, X.; Woo, A. Y. Y.; Borau-Garcia, J.; Baumgartner, T., *Chem. Eur. J.* **2013**, *19*, 7620–7630; b) Ren, Y.; Biegger, F.; Baumgartner, T., *J. Phys. Chem. C* **2013**, *117*, 4748–4758; c) Huynh, H. V.; He, X.; Baumgartner, T., *Chem. Commun.* **2013**, *49*, 4899–4901; d) Ishidoshiro, M.; Imoto, H.; Tanaka, S.; Naka, K., *Dalton Trans.* **2016**, *45*, 8717–8723; e) Macdonald, C. L. B.; Binder, J. F.; Swidan, A. a.; Nguyen, J. H.; Kosnik, S. C.; Ellis, B. D., *Inorg. Chem.* **2016**, *55*, 7152–7166; f) Beldjoudi, Y.; Osorio-Roman, I.; Nascimento, M. A.; Rawson, J. M., *J. Mat. Chem. C* **2017**, *5*, 2794–2799; g) Green, J. P.; Cryer, S. J.; Marafie, J.; White, A. J. P.; Heeney, M., *Organometallics* **2017**, *36*, 2632–2636.

(15) see CSD codes: OWIJOU, OWIJUA, REPREL, REPSAI.

(16) Melhuish, W. H., *J. Phys. Chem.* **1961**, *65*, 229–235.

(17) Stoll, S.; Schweiger, A., *J. Magn. Reson.* **2006**, *178*, 42–55.

(18) Frisch, M. J.; Trucks, G. W.; Schlegel, H. B.; Scuseria, G. E.; Robb, M. A.; Cheeseman, J. R.; Scalmani, G.; Barone, V.; Mennucci, B.; Petersson, G. A.; Nakatsuji, H.; Caricato, M.; Li, X.; Hratchian, H. P.; Izmaylov, A. F.; Bloino, J.; Zheng, G.; Sonnenberg, J. L.; Hada, M.; Ehara, M.; Toyota, K.; Fukuda, R.; Hasegawa, J.; Ishida, M.; Nakajima, T.; Honda, Y.; Kitao, O.; Nakai, H.; Vreven, T.; Montgomery Jr., J. A.; Peralta, J. E.; Ogliaro, F.; Bearpark, M. J.; Heyd, J.; Brothers, E. N.; Kudin, K. N.; Staroverov, V. N.; Kobayashi, R.; Normand, J.; Raghavachari, K.; Rendell, A. P.; Burant, J. C.; Iyengar, S. S.; Tomasi, J.; Cossi, M.; Rega, N.; Millam, N. J.; Klene, M.; Knox, J. E.; Cross, J. B.; Bakken, V.; Adamo, C.; Jaramillo, J.; Gomperts, R.; Stratmann, R. E.; Yazyev, O.; Austin, A. J.; Cammi, R.; Pomelli, C.; Ochterski, J. W.; Martin, R. L.; Morokuma, K.; Zakrzewski, V. G.; Voth, G. A.; Salvador, P.; Dannenberg, J. J.; Dapprich, S.; Daniels, A. D.; Farkas, Ö.; Foresman, J. B.; Ortiz, J. V.; Cioslowski, J.; Fox, D. J. *Gaussian 09*, Gaussian, Inc.: Wallingford, CT, USA, 2009.

(19) Becke, A. D., *J. Chem. Phys.* **1993**, *98*, 5648–5652.

(20) Ditchfield, R.; Hehre, W. J.; Pople, J. A., *J. Chem. Phys.* **1971**, *54*, 724–728.

(21) a) Hay, P. J.; Wadt, W. R., *J. Chem. Phys.* **1985**, *82*, 270–283; b) Wadt, W. R.; Hay, P. J., *J. Chem. Phys.* **1985**, *82*, 284–298; c) Hay, P. J.; Wadt, W. R., *J. Chem. Phys.* **1985**, *82*, 299–310.

(22) Yanai, T.; Tew, D. P.; Handy, N. C., *Chem. Phys. Lett.* **2004**, *393*, 51–57.

(23) Hanwell, M. D.; Curtis, D. E.; Lonie, D. C.; Vandermeersch, T.; Zurek, E.; Hutchison, G. R., *J. Cheminform.* **2012**, *4*, 17.

(24) a) Perdew, J. P.; Ernzerhof, M.; Burke, K., *J. Chem. Phys.* **1996**, *105*, 9982–9985; b) Adamo, C.; Barone, V., *J. Chem. Phys.* **1999**, *110*, 6158–6170.

(25) Neese, F., Wiley Interdisciplinary Reviews: Computational Molecular Science **2012**, 2, 73–78.

(26) Weigend, F.; Ahlrichs, R., *Phys. Chem. Chem. Phys.* **2005**, *7*, 3297–3305.

(27) Neese, F., *J. Chem. Phys.* **2005**, *122*, 034107.